OAK RIDGE NATIONAL LABORATORY
MANAGED BY UT-BATTELLE FOR THE DEPARTMENT OF ENERGY

ORNL/TM-2011/360

Reference Inflow Characterization for River Resource Reference Model: Reference Model 2 (RM2)

October 2011

Prepared by

Vincent S. Neary, Ph.D., P.E.

UT-BATTELLE

DOCUMENT AVAILABILITY

Reports produced after January 1, 1996, are generally available free via the U.S. Department of Energy (DOE) Information Bridge.

Web site http://www.osti.gov/bridge

Reports produced before January 1, 1996, may be purchased by members of the public from the following source.

National Technical Information Service
5285 Port Royal Road
Springfield, VA 22161
Telephone 703-605-6000 (1-800-553-6847)
TDD 703-487-4639
Fax 703-605-6900
E-mail info@ntis.gov
Web site http://www.ntis.gov/support/ordernowabout.htm

Reports are available to DOE employees, DOE contractors, Energy Technology Data Exchange (ETDE) representatives, and International Nuclear Information System (INIS) representatives from the following source.

Office of Scientific and Technical Information
P.O. Box 62
Oak Ridge, TN 37831
Telephone 865-576-8401
Fax 865-576-5728
E-mail reports@osti.gov
Web site http://www.osti.gov/contact.html

ORNL/TM-2011/360

Environmental Science Division

Reference Inflow Characteristics for River Resource Reference Model: Reference Model 2 (RM2)

Vincent S. Neary, Ph.D., P.E.

Date Published: October 2011

Prepared by
OAK RIDGE NATIONAL LABORATORY
Oak Ridge, Tennessee 37831-6283
managed by
UT-BATTELLE, LLC
for the
U.S. DEPARTMENT OF ENERGY
under contract DE-AC05-00OR22725

TABLE OF CONTENTS

ABSTRACT

Sandia National Laboratory (SNL) is leading an effort to develop reference models for marine and hydrokinetic technologies and wave and current energy resources. This effort will allow the refinement of technology design tools, accurate estimates of a baseline levelized cost of energy (LCoE), and the identification of the main cost drivers that need to be addressed to achieve a competitive LCoE. As part of this effort, Oak Ridge National Laboratory was charged with examining and reporting reference river inflow characteristics for reference model 2 (RM2). Published turbulent flow data from large rivers, a water supply canal and laboratory flumes, are reviewed to determine the range of velocities, turbulence intensities and turbulent stresses acting on hydrokinetic technologies, and also to evaluate the validity of classical models that describe the depth variation of the time-mean velocity and turbulent normal Reynolds stresses. The classical models are found to generally perform well in describing river inflow characteristics. A potential challenge in river inflow characterization, however, is the high variability of depth and flow over the design life of a hydrokinetic device. This variation can have significant effects on the inflow mean velocity and turbulence intensity experienced by stationary and bottom mounted hydrokinetic energy conversion devices, which requires further investigation, but are expected to have minimal effects on surface mounted devices like the vertical axis turbine device designed for RM2. A simple methodology for obtaining an approximate inflow characterization for surface deployed devices is developed using the relation $u_{max}=(7/6)V$ where V is the bulk velocity and u_{max} is assumed to be the near-surface velocity. The application of this expression is recommended for deriving the local inflow velocity acting on the energy extraction planes of the RM2 vertical axis rotors, where $V=Q/A$ can be calculated given a USGS gage flow time-series and stage vs. cross-section area rating relationship.

INTRODUCTION

Site velocity and turbulence information over the energy extracting plane of the reference model 2 (RM2) vertical axis turbine shown in Figure 1 is required for determining design and performance characteristics, estimates of annual energy production (AEP), and estimates of levelized cost of energy (LCoE). As shown in Figure 1, the velocity and turbulence can vary considerably over the flow depth in a river channel, as well as over the extraction plane of the marine and hydrokinetic (MHK) energy converter machine. In addition, rivers can have extreme variations in flow and stage, and measurements on the order of several decades are typically required to obtain meaningful statistics describing flow variability. It is impractical for instrument deployments to span the return periods found in rivers due to instrument limitations and prohibitive costs. Alternatively, classical models developed from laboratory experiments to describe velocity and turbulence profiles in open channel flows may be used to characterize river hydrokinetic resources. These classical models have recently been validated

for large rivers (Neary and Sale 2010). These models include the power and logarithmic laws for the vertical mean velocity profile of a flat plate turbulent boundary layer flow (White 1974) and exponential decay models developed by Nezu and Nakagawa (1993) for normal Reynolds stresses of depth-limited boundary shear flows in open channel flumes.

These classical models assume steady uniform flow, but unregulated rivers and tidal channels exhibit great variability of discharge and depth over time scales varying from minutes to days. The discharge of regulated rivers, such as tailwaters below hydropower dams, can change within minutes, but exhibit less depth and flow variability than regulated rivers. Figure 3 shows daily discharge and stage data on the Missouri River for an approximately twenty year period. The discharge at this site varies over three orders of magnitude, and the stage varies from approximately 1 to 30 m. Also, both unregulated and regulated rivers are rarely uniform along their reaches. Channel geometry, roughness, mean-section depth and bulk velocity typically change along the longitudinal direction. In addition to challenges in characterizing the variations of bulk (section averaged) flow properties, the local mean flow properties of rivers can be highly three-dimensional as a result of variations in river alignment and vortex shedding from in-stream structures. Pressure gradients associated with nonuniform surface profiles cause significant departures in the wake region. Wind shear on the water surface also can cause significant departures from semi-theoretical models that estimate mean velocity and Reynolds stress profiles.

In this report the work by Neary and Sale (2010) is reviewed and used to provide a methodology for a first order approximation for river resource inflow characterization for the RM2.

METHODS

Neary and Sale (2010) reviewed published turbulent flow data from large rivers and tidal channels, as well a water supply canal and laboratory flumes, to evaluate the application of classical models that describe the depth variation of the time-mean velocity and turbulent normal Reynolds stresses. Large rivers were defined as those having a depth of at least one meter and velocities exceeding 1 m/s. This criterion significantly limited the data reviewed, but these large rivers with fast currents are characteristic of the sites being targeted by the MHK industry.

McQuivey (1973) measured mean velocity and turbulence profiles along reaches of the Missouri River downstream of Omaha, NE, the Mississippi River upstream of Vicksburg, MS, the Rio Grande conveyance channel near the intersection of Interstates 60 and 85 in New Mexico, and a large laboratory flume at Colorado State University. At these sites, mean velocity was first measured with a modified propeller meter, and then turbulence was measured with a hot film anemometer moved to the same location as the propeller meter. At the Missouri and Mississippi Rivers, the propeller meter and hot film instruments were suspended from a cable

off the side of a boat, and measurements were conducted at several transverse locations across the channels. Measurements in the Missouri and Mississippi Rivers were conducted at several different times and discharges. Bedforms consisted of dunes and flat conditions, and no influence from flow unsteadiness was reported at the Missouri and Mississippi River sites. At the Rio Grande conveyance channel, measurements were taken along channel centerline and the shallower depth permitted several propeller meters to be mounted simultaneously to a wading rod. Measurements at the Rio Grande canal were conducted during two different times: one at which large and mobile sand bedforms were present, and during the other condition the sand bed was flat. The laboratory flume was 61m long with a rectangular cross section 2.44m wide by 1.22m deep, and included sections with sand dunes and flat sand beds. The measurements reported herein were taken along the flume centerline 36.6m downstream from the headbox, and at two different discharges.

Holmes and Garcia (2008) reported turbulence measurements for a reach of the Missouri River, near St. Charles, Missouri using an acoustic Doppler velocimeter mounted to a sediment sampler suspended from a boat (Figure 3). This site on the Missouri River was fairly straight with sand dune height to water-depth ratios from 1/6 to 1/7, and the measurements were conducted during quasi steady flow conditions when the flow was well within the channel banks. Nikora and Smart (1997) measured turbulence with electronic Pitot tubes on the gravel-bed Hurunui River, New Zealand in the proximity of a bridge. Although these measurements on the Hurunui River were taken during the falling stage of a flood, Nikora and Smart showed that the unsteady effects would not have strongly influenced their turbulence measurements. Carling et al. (2002) measured velocity on River Severn, England during periods of over-bank flow on a nearly straight and deep gravel bed channel downstream of a double-meandering channel bend. The mean velocity profiles reported herein from the River Severn were conducted with a boat-deployed directional current meter over the thalweg, and the flow could be considered quasi steady over the specific period of time of data collection.

Velocity profiles from the reviewed data sets were further screened by inspection. By applying the log-law (Nezu & Nakagawa 1993) which describes the vertical distribution of longitudinal velocity in open channel flows with rough boundaries,

$$\frac{\bar{u}}{u_*} = \frac{1}{\kappa}\ln\left(\frac{z}{k_s}\right) + 8.5,$$

the authors computed the shear velocity, $u_* = \sqrt{\tau_o/\rho}$, from the slope of the best fit line through the time averaged vertical velocity profile. With the exception of the Holmes & Garcia data set, many of the reviewed vertical profiles contained only one or two data points in the wall region (z/D < 0.2) where the log law applies. For these cases, data from the entire vertical profile was used in this fitting method for calculating the shear velocity. Results for shear velocity using this method compared well with the values reported by the original investigators,

and also calculated by McQuivey (1973), in which the shear velocity was determined using the relationship $u_* = \sqrt{gRS}$, which is less accurate (Biron et al. 1998). Profiles with significant non-monotonic behavior due to 3D flow effects or vortex shedding were eliminated. This non-monotonic behavior was identified when the fitting procedure for the shear velocity resulted in a poor coefficient of determination, R^2; thus any profiles with R^2 values less than 0.8 were discarded. Of the velocity profiles reviewed, 13% were eliminated because they exhibited non-monotonic behavior or could not be well represented by the log law.

The final dataset included 39 profiles. Bulk flow properties for these open channel flows are summarized in Table 1. All Reynolds numbers are above 400,000 and Froude numbers indicate subcritical flows for all measurements with the maximum Froude number occurring for the Hurunui River in New Zealand (Nikora & Smart 1997).

Table 1. Bulk flow properties of reviewed open channel flow data

investigators	site	Q_m	Q^*	$D_{avg}{}^*$	W^*	Re^{**}	Fr^{**}
		(m^3/s)	(m^3/s)	(m)	(m)	(10^6)	
McQuivey (1973)	Mississippi	19000[a]	7900-9200	7.4-16	570-890	3-9	0.06-0.17
McQuivey (1973)	Missouri	910[b]	890-920	2.9-3.1	200-210	4-38	0.19-0.35
Holmes & Garcia (2008)	Missouri	2200[c]	1400	4.9	350-400	5-9	0.13-0.17
McQuivey (1973)	Rio Grande canal	NR	14-26	0.85-0.91	21-22	0.8-1.3	0.36-0.49
Nikora & Smart (1997)	Hurunui	NR	250	1.2	85-90	1-5	0.70-0.79
Carling et al. (2002)	Severn	NR	100	NR	NR	3-6	0.10-0.16
McQuivey (1973)	CSU flume	NR	1-2	0.33-0.53	2.44	0.4-0.8	0.69-0.74

NR = not reported

* reported by original investigators at time of measurement

** derived by authors, using depth averaged velocity and local water depth

[a] mean annual discharge from nearest USGS station #07289000, record period: 2009

[b] mean annual discharge from nearest USGS station #06610000, record period: 1953-2009

[c] mean annual discharge from nearest USGS station #06935965, record period: 2001-2010

Turbulence is characterized by velocity and vorticity fluctuations about all three components of the mean velocity and vorticity in a statistically steady mean flow so that the instantaneous velocity at any point for any instant in time can be decomposed into the mean (Reynolds-averaged) velocity (vorticity) and the velocity (vorticity) fluctuation (See Tennekes and Lumley 1992 for details). In contrast, for laminar flows there is no departure of the instantaneous velocity from the mean velocity for a statistically steady mean flow. Fluid parcels in which the fluctuations are correlated can broadly be defined as coherent motions and are generally thought to be a result of eddies or vortices that have directly been observed in flow visualization experiments of turbulent flows (e.g. Van Dyke 1982). The time scales, or duration over which turbulent eddies disrupt the steady mean flow, exhibit great variation from small

(i.e., Kolmogorov (temporal) microscale = $\sqrt{\nu/\varepsilon}$) to large (i.e., convective time-scale = $L/\overline{u}_i$), where ν is the kinematic viscosity in system international (SI) units m^2/s, ε (m^2/s^3) is the energy dissipation rate per unit mass, *L* (m) is a characteristic length scale of the channel bounding geometry (e.g., flow depth) and $\overline{u}_i$ (m/s) is a characteristic mean velocity. The smallest scale in a turbulent flow is limited by the fluid viscosity and is estimated by the Kolmogorov (spatial) microscale, $\eta = (\nu^3/\varepsilon)^{1/4}$, while the largest scale is characterized by *L.* The Reynolds number, $R = \overline{u}_i L/\nu$, which is a measure of the inertial to viscous forces acting on a fluid parcel, governs the onset of turbulence and the amount of small eddies between the □ and *L* (p. 102, Van Dyke 1982), which cause increased turbulence intensity.

The study adopts Reynolds averaging to decompose an instantaneous velocity component in to its mean velocity and turbulent fluctuation

$$u_i = \overline{u_i} + u_i'$$

Substituting this into the Navier-Stokes equation, which represents the conservation of momentum for a fluid element at any instant in time and time-averaging produces the Reynolds-averaged-Navier-Stokes equation

$$\rho \frac{\partial \overline{u}_i \overline{u}_j}{\partial x_j} = \rho g_i - \overline{f}_i + \frac{\partial}{\partial x_j}\left[- p\delta_{ij} + \mu\left(\frac{\partial \overline{u}_i}{\partial x_j} + \frac{\partial \overline{u}_j}{\partial x_i} \right) - \rho \overline{u_i' u_j'} \right]$$

This equation states that the rate change of momentum of a fluid element per unit volume is balanced by the forces per unit volume acting on the fluid element. Forces on the right hand side of the equation include the gravitational body force, the drag force, and in brackets, the isotropic hydrostatic pressure force, viscous stresses, which are negligible outside the viscous sublayer, and the Reynolds or apparent stresses due to turbulence. The Reynolds stress tensor is symmetric and includes six terms, three normal stresses along the diagonal, and the three non-diagonal terms, which are shear stresses

$$\begin{bmatrix} \rho\overline{u'u'} & \rho\overline{u'v'} & \rho\overline{u'w'} \\ & \rho\overline{v'v'} & \rho\overline{v'w'} \\ & & \rho\overline{w'w'} \end{bmatrix}$$

The square root of the normal stresses divided by the density, $\sqrt{\overline{u'u'}}$, $\sqrt{\overline{v'v'}}$, $\sqrt{\overline{w'w'}}$, are the longitudinal, transverse and vertical turbulence intensities. For turbulent boundary layer flows, if the dominant flow direction is longitudinal, then the longitudinal turbulence intensity is the dominant intensity. In the wind energy industry, the percentage of this term with respect to the local longitudinal mean velocity $\overline{u}$ at the centerline of the energy extraction plane (hub

height for horizontal axis turbines) is used to characterize the turbulence of the inflow for wind turbine design.

RESULTS

Velocity and Turbulence Distributions and Magnitudes

As expected, the mean velocity $\bar{u}$ is lowest near the channel bottom and increases as it approaches the free water surface $z=D$ (Figure 4a). The maximum $\bar{u}$ is usually near the free water surface. Maximum $\bar{u}$ values range from 1 to 4 m/s and depths z from 1 to 35 m for the data reviewed. Given that flow measurements for the Mississippi River by McQuivey (1973) were taken when the flow was well below the mean annual discharge Q_m (Table 1), one would expect higher maximum $\bar{u}$ at higher z and flows $Q>Q_m$. Figure 4b shows the corresponding longitudinal turbulence intensity profiles. These also follow known trends with an exponential increase from the free water surface to the near wall region. When comparing the velocity and turbulence profiles in Figure 4, one observes that the longitudinal turbulence intensity $\sqrt{\overline{u'u'}}$ ranges from approximately 0.05 to 0.5 m/s, and increases with $\bar{u}$. The no-slip condition requires that the turbulence intensity, and all components of the Reynolds stress tensor, is zero at the bottom of a fixed boundary, but field measurements are currently limited within the near wall region, even with state-of-the-art hydroacoustic instruments, and rivers typically have mobile beds with a non-zero mean velocity and Reynolds stresses. The minimum and maximum range of elevations for measurements by McQuivey, Holmes and Garcia, Nikora and Smart, and Carling et al. were z/D=0.03-0.91, 0.02-0.96, 0.27-0.93 and 0.06-0.77, respectively.

Longitudinal turbulence intensity profiles with z normalized by the flow depth D are shown in Figure 5. The turbulence intensity $\sqrt{\overline{u'u'}}$ is normalized by the local mean velocity $\bar{u}$ and multiplied by 100 to determine the turbulence intensity percentage with respect to the local mean velocity; a common way to non-dimensionalize turbulence intensity in the wind-energy industry for wind resource characterization. The turbulence intensity $\sqrt{\overline{u'u'}}$ is plotted on a logarithmic scale to show the large variation if turbulence. The plot shows that extreme values of turbulence intensity typically occur very close to the bed. When non-dimensionalized by the local $\bar{u}$, $\sqrt{\overline{u'u'}}$ increases exponentially from the free water surface z/D=1 into the near wall region z/D<0.1, but the large scatter indicates that $\sqrt{\overline{u'u'}}$ does not scale with $\bar{u}$ to develop a simple one-to-one empirical relationship.

Comparison with Classical Models

Field measurements of $\bar{u}$ are non-dimensionalized by $\bar{u}_{\max}$ in Figure 6 with the power law equation

$$\frac{\bar{u}}{\bar{u}_{\max}} = \left(\frac{z}{D}\right)^{1/\alpha}$$

Based on the power law assumption, $\bar{u}_{\max}$ occurs at the surface (z/D = 1), but the measured data shows that $\bar{u}_{\max}$ can occur beneath the surface due to wind, wave and three-dimensional flow effects.

The power law exponent $1/\alpha$ was observed to vary from 1/3 to 1/12 between individual profiles, with a best fit value of 1/5.4 through all the data. Variation in the exponent can be attributed to a number of causes, including measurement error, pressure gradients, roughness and three-dimensional flow effects. The significant differences between the exponents would translate in to more significant errors in drag and power acting on the energy extraction plane since drag and power are proportional to $\bar{u}$ to the second and third powers.

Field measurements of normal stresses, e.g. $\sqrt{\overline{u'u'}}$, normalized by shear velocity $u_* = \sqrt{\tau_o/\rho}$ are compared in Figure 7 with the exponential decay models developed by Nezu and Nakagawa (1993) for steady uniform flow in smooth laboratory flumes

$$\sqrt{\overline{u'u'}}/u_* = 2.30\exp(-z/D)$$
$$\sqrt{\overline{v'v'}}/u_* = 1.63\exp(-z/D)$$
$$\sqrt{\overline{w'w'}}/u_* = 1.27\exp(-z/D)$$

These expressions are universal for smooth boundaries between (0.1-0.2)< z/*D*<0.9, independent of Reynolds and Froude number, and show that $\sqrt{\overline{u'u'}}/u_* > \sqrt{\overline{v'v'}}/u_* > \sqrt{\overline{w'w'}}/u_*$. They do not apply near the wall approximately z/*D*<(0.1 to 0.2) as the no slip condition requires turbulence intensities to decrease from a maximum value to zero at z/*D*=0. Nor do they apply in the free surface region above z/*D*<0.9, where $\sqrt{\overline{w'w'}}/u_*$ is damped. A peak value of $\sqrt{\overline{u'u'}}/u_*$ =2.8 is observed in the near-wall region in wall coordinates at z+=17, where $z^+ = zu_*/\nu$ (Nezu and Nakagawa 1993). A peak in $\sqrt{\overline{u'u'}}/u_*$ could not be observed in any of the data reviewed because the measurements were not taken close enough to the bed.

The comparison indicates that the field measurements are in reasonable agreement with the exponential decay models developed from laboratory flumes, although there is considerable scatter. Measurement error as well as complex hydrodynamic effects summarized above are

possible causes. The measurements by Holmes and Garcia (2008) are the only measurements known by the authors of the normal Reynolds stresses $\sqrt{\overline{v'v'}}/u_*$ and $\sqrt{\overline{w'w'}}/u_*$ in large rivers (depths > 1 m and currents > 1m/s). These turbulence measurements are in fair agreement with the exponential decay models, except near the surface where the models underestimate the data. Field measurements near the free water surface, however, are likely prone to error from wave motion and wind shear effects.

Effects of Depth Variability

The effects of large depth variability on the location of the energy extraction area and its centerline relative to the velocity and turbulence characteristic profiles are shown in Figure 8. Two river hydrokinetic devices at sites with a large range of depth variability are compared to a tidal site where depth variability is not nearly as large. The centerline and height of the energy extraction plane is also non-dimensionalized with *D*, which causes the centerline and height to decrease with greater depth. In theory, the normalized velocity and turbulence distributions would remain unchanged with depth and flow changes. Therefore, Figure 8 illustrates the additional variation in velocity and turbulence that a device will experience over its design life as a result of moving up and down the relative depth *z*/*D*.

DISCUSSION

For the data set examined by Neary and Sale (2010), only 13% of the large river profiles were non-monotonic because of the hydrodynamic complexities of rivers, such as secondary circulation. Of those that did exhibit monotonic behavior and fit the log law well, no universal exponent for the power law model was observed and considerable scatter was observed around the best fit line with the exponent of 1/5.4. This value is close to the theoretical value for flat plate boundary layer shear flows, 1/7, and the theoretical value derived from Manning's equation, 1/6, (Appendix I).

Near the free surface, where the RM2 VAT would be deployed, velocities between 1-2 m/s are observed for large sinuous canaliform rivers like the Mississippi and Missouri Rivers; and longitudinal turbulence intensities are approximately 10 %. As noted by Neary and Sale (2010), depth and flow variability present challenges for characterizing river resources for fixed or bottom mounted MHK machines. Surface deployed turbines like the RM2 VAT, however, will typically be sampling near maximum velocities at the free surface.

CONCLUSION

Accounting for the reduced accuracy of velocity and turbulence measurements in large rivers and the uncertainty in calculation of the shear velocity, the reviewed turbulence measurements coincide fairly well with the semi-theoretical equations developed by Nezu and Nakagawa (1993). Although significant scatter is seen in the data, it is encouraging that the velocity and turbulence measurements clearly follow the trends of the logarithmic, power law and

exponential decay models. This shows that these classical flow models can be used to provide coarse estimates of the vertical distribution of velocity and turbulence magnitudes in large rivers and should be adopted for the river inflow characterization model for RM2.

The derivation in the Appendix I shows that , $u_{max}=(7/6)V$ is a reasonable assumption and independent of the shear velocity. The application of this expression is recommended for deriving the local inflow velocity acting on the EEP of the RM2 VAT, where $V=Q/A$ can be calculated given a USGS gage flow time-series and stage vs. cross-section area rating relationship.

ACKNOWLEDGMENTS

The author thanks the Office of Energy Efficiency and Renewable Energy (EERE) of the Department of Energy (DOE) who provided funding for this review under DOE Contract DE-AC05-00OR22725. The authors also thank Bob Holmes of the United States Geological Survey for providing velocity and turbulence measurement data he collected on the Missouri River.

NOTATION

$\overline{u}_{\max}$	=	maximum longitudinal time-averaged velocity in vertical profile, m s^{-1}
u_*	=	shear velocity, $\sqrt{\tau_o/\rho}$, m s^{-1}
τ_o	=	bed shear stress, N m^{-2}
κ	=	Von Kármán constant
k_s	=	characteristic roughness length scale, m
g	=	gravitational acceleration constant, m s^{-2}
P	=	wetted perimeter, m
A	=	flow section area, m^2
R	=	hydraulic radius, A/P, m
S	=	water slope
Q	=	discharge, m^3 s^{-1}
Q_m	=	mean annual discharge, m^3 s^{-1}
W	=	local channel width, m
D	=	local water depth, m
D_{avg}	=	cross sectional average water depth, m
Re	=	Reynolds number, $\frac{U_{Davg}D}{\nu}$
Fr	=	Froude number, $\frac{U_{Davg}}{\sqrt{gD}}$
U_{Davg}	=	depth averaged longitudinal velocity, m s-1
u,v,w	=	instantaneous longitudinal, lateral, and vertical velocities, m s^{-1}
$\overline{u}, \overline{v}, \overline{w}$	=	time-averaged longitudinal, lateral, and vertical velocities, m s^{-1}
u',v',w'	=	instantaneous longitudinal, lateral, and vertical fluctuating velocities, m s^{-1}
$\sqrt{\overline{u'u'}}, \sqrt{\overline{v'v'}}, \sqrt{\overline{w'w'}}$	=	standard deviation of the longitudinal, lateral, and vertical velocities, m s^{-1}
x, y, z	=	longitudinal, lateral, and vertical coordinate distance, m
$\overline{f}$	=	body force per unit volume of fluid, N m^{-3}
p	=	isotropic hydrostatic pressure force, N m^{-2}
ρ	=	fluid density, kg m^{-3}
ν	=	kinematic viscosity, m^2 s^{-1}
μ	=	dynamic viscosity, N s m^{-1}
α	=	power law exponent ($1/\alpha$)

REFERENCES

Biron, P. M., Lane, S. N., Roy, A. G., Bradbrook, K. F. and Richards, K. S. (1998), Sensitivity of bed shear stress estimated from vertical velocity profiles: the problem of sampling resolution. Earth Surface Processes and Landforms, 23: 133–139. doi: 10.1002/(SICI)1096-9837(199802)23:2<133::AID-ESP824>3.0.CO;2-N

Carling, P. A., Z. Cao, M. J. Holland, D. A. Ervine, and K. Babaeyan-Koopaei (2002), Turbulent flow across a natural compound channel, *Water Resour. Res.*, *38*(12), 1270.

Clarke, R.T. (2007). Hydrological prediction in a non-stationary world. *Hydrol. Earth Syst. Sci*., 11(1), 408-414.

Holmes, R.R. and Garcia, M.H. (2008). Flow over bedforms in a large sand-bed river: A field investigation. *Journal of Hydraulic Research*, 46(3): p. 322-333.

Lima C.H.R. and Lall U. (2010). Spatial scaling in a changing climate: A hierarchical bayesian model for non-stationary multi-site annual maximum and monthly streamflow, *Journal of Hydrology*, 383, 307–318.

McQuivey, R.S., *Summary of Turbulence Data from Rivers, Conveyance Channels, and Laboratory Flumes*. USGS Report 802-B Turbulence in Water, 1973.

Neary, V.S. and Sale, D.C. (2010) "Flow characteristics of river resources for hydrokinetic energy conversion." *Conf. Proc.*, *HydroVision International*, July 27-30, 2010, Charlotte, NC.

Nezu, I. and Nakagawa, H. *Turbulence in Open-Channel Flows*, A.A. Balkema, Rotterdam, 1993.

Nikora, V.I. and Smart, G.M., (1997). Turbulence characteristics of New Zealand gravel-bed rivers. *Journal of Hydraulic Engineering*. 123(9): p. 764-773.

White, F.M., Viscous Fluid Flow, McGaw-Hill. 1974.

APPENDIX I

Given a power-law velocity distribution in a very wide open channel in uniform flow is given by

$$\frac{u}{u_*} = a\left(\frac{z}{k_s}\right)^m$$

where u is the point velocity; u_* is the shear velocity; a is a constant; z is the distance above the channel bed; k_s is the equivalent sand-grain roughness; and m is the given fractional exponent that is constant.

Integrate the point velocity distribution to find the mean velocity:

$$V = \frac{1}{y_0}\int_0^{y_0} au_*\left(\frac{z}{k_s}\right)^m \mathrm{d}z = \frac{au_*}{(m+1)y_0}\left(\frac{y_0}{k_s}\right)^{m+1} k_s$$

$$V = \frac{au_*}{(m+1)}\left(\frac{y_0}{k_s}\right)^m$$

The maximum velocity occurs at $z = y_0$, and is given by

$$u_{\max} = au_*\left(\frac{y_0}{k_s}\right)^m$$

Comparing the expressions for V and $u_{\max}$, we have

$$V = \frac{u_{\max}}{m+1}$$

Rewrite the expression for mean velocity, substituting $u_* = (gy_0S)^{1/2}$, to obtain

$$V = \frac{a\sqrt{g}}{(m+1)k_s^m} y_0^{m+1/2} S^{1/2}$$

If ***m* = 1/6**, note that this equation for V agrees with Manning's and Strickler's equations in the exponents on y_0, k_s, and S. In other words, Manning's equation is compatible with a 1/6 power law velocity distribution. **Therefore, u_{max}=*(7/6)V* is a reasonable assumption and is independent of the shear velocity.**

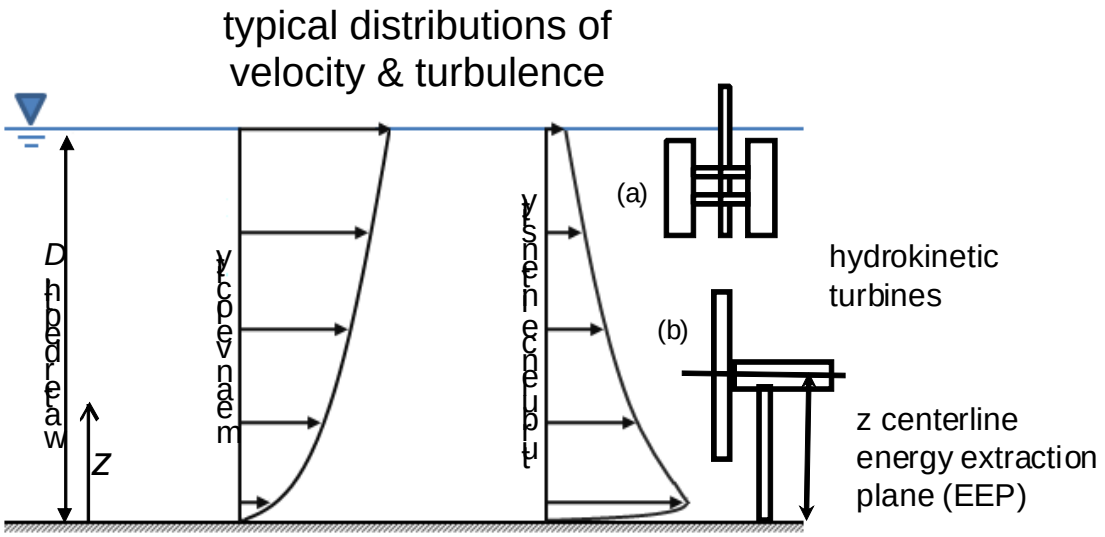

Figure 1. Typical distributions of velocity and turbulence and sketch of (a) surface mounted vertical axis turbine; and (b) bottom mounted horizontal-axis turbine.

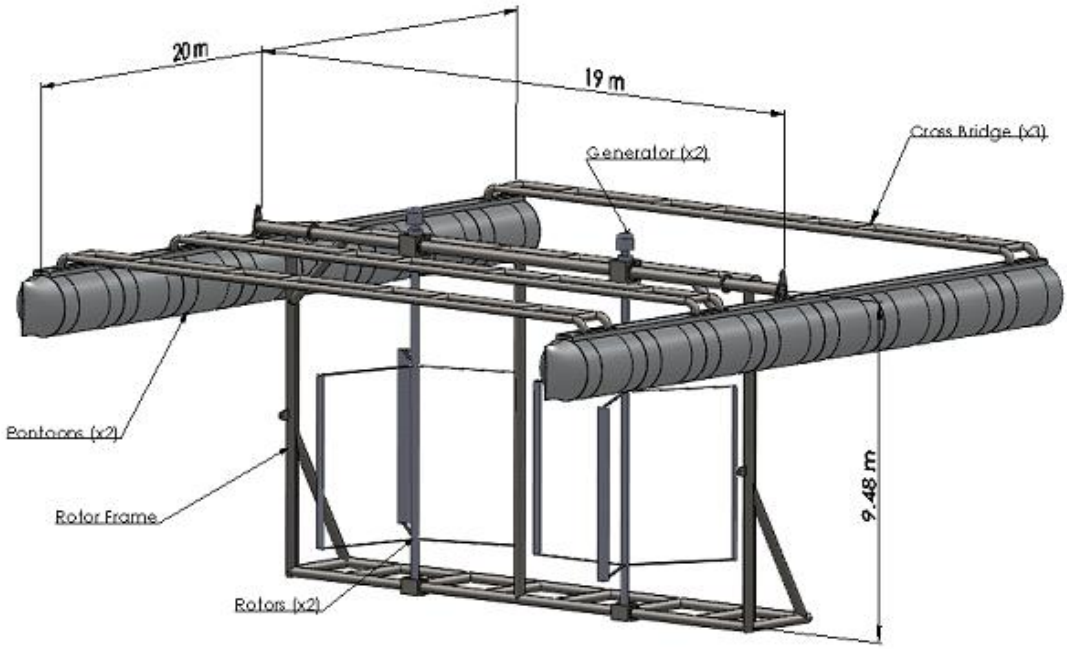

Figure 2. Vertical axis turbine for RM2 (Personnel communication, Matt Barone 2011).

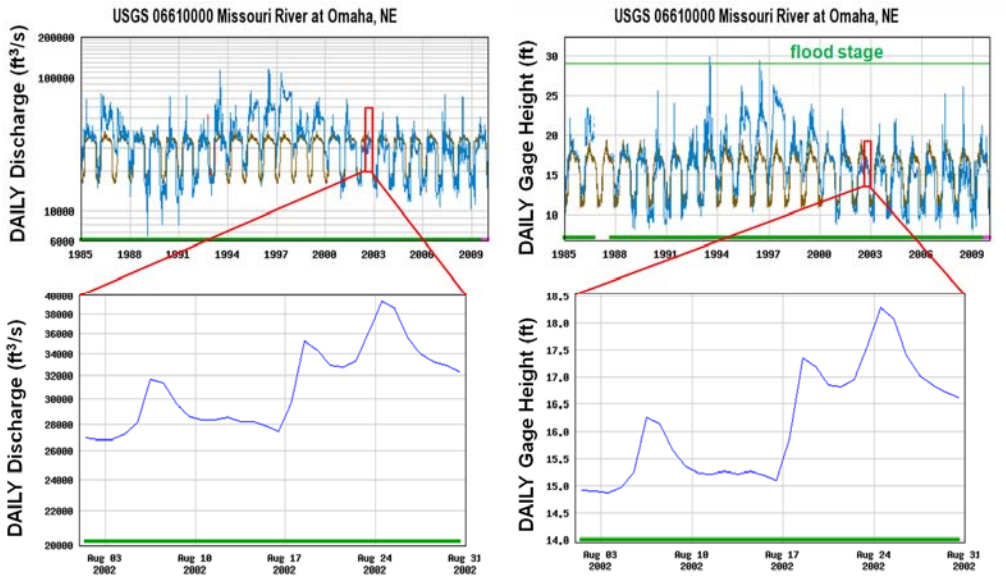

Figure 3. Daily flow and depth time-series record for approximately twenty-year period of record (POR) on the Missouri River, Nebraska (USGS 06610000). Blue indicates the daily values. Brown indicates the daily mean values for the (POR). The inset plots show the flow and depth time series during field measurements by Holmes and Garcia (2009).

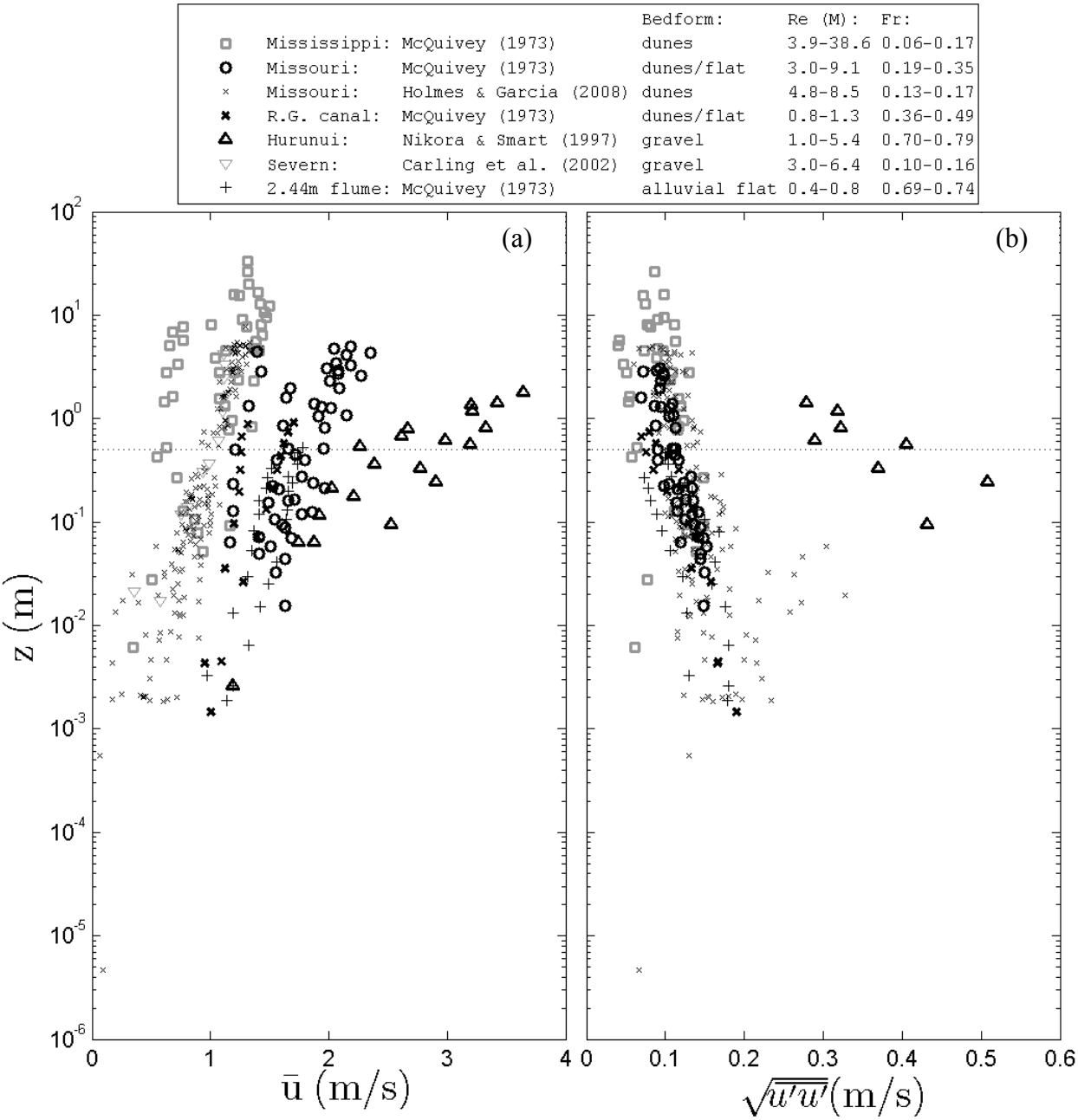

Figure 4. (a) Mean longitudinal velocity profiles. (b) Longitudinal turbulence intensity profiles. The dashed horizontal line indicates z = 0.5 m. HKEC devices will typically operate at depths greater than 0.5m off the bed.

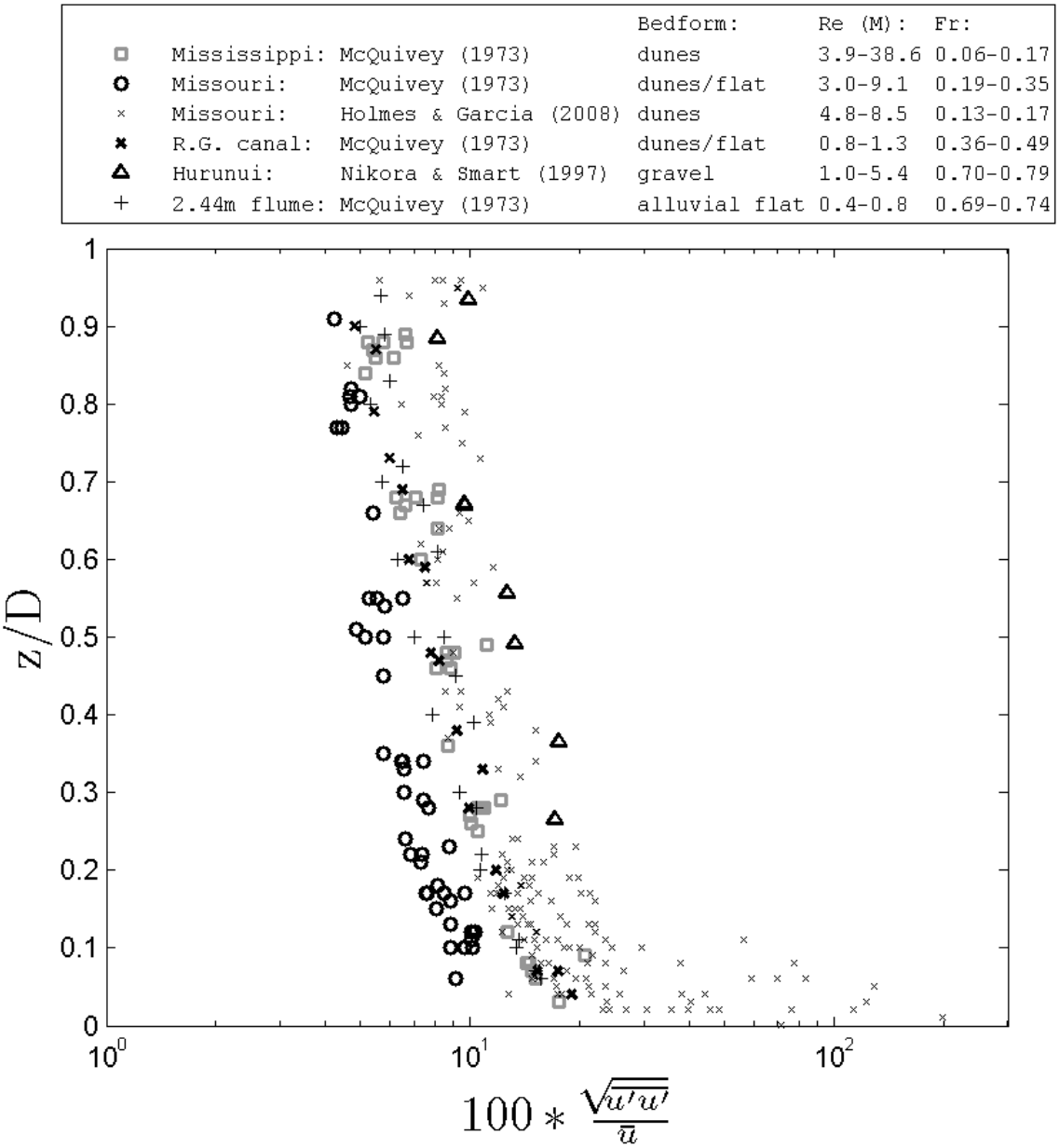

Figure 5. Longitudinal turbulence intensity profiles with z normalized by the flow depth and the turbulence intensity normalized by the local mean velocity and multiplied by 100 to determine the percentage of turbulence intensity with respect to the local mean velocity.

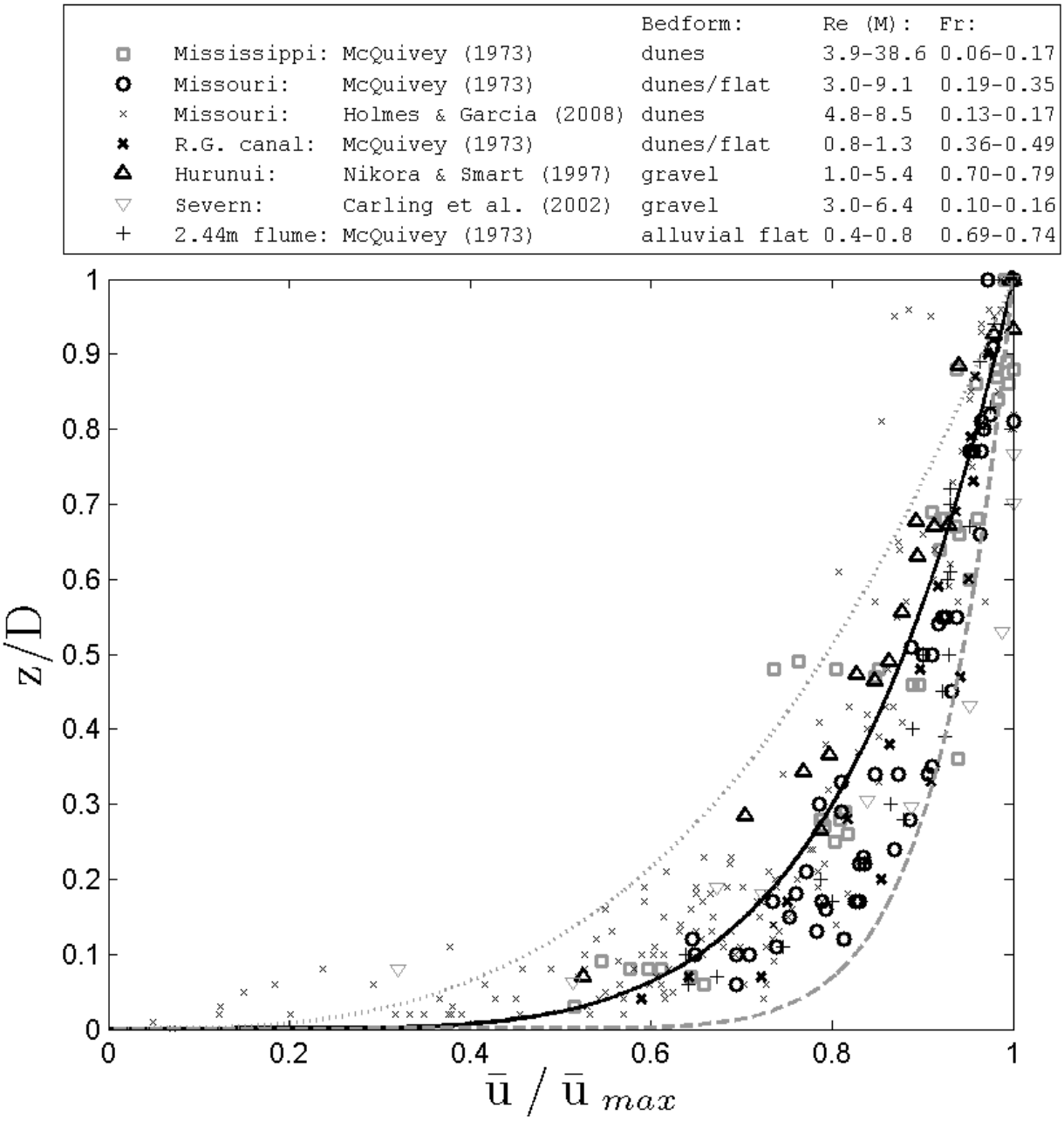

Figure 6. Power law velocity profiles with z normalized by D and $\bar{u}$ normalized by $\bar{u}_{\max}$. The solid black line represents the best fit of the power law with exponent $1/\alpha$ through the data, and the resulting best fit $\alpha = 5.4$ ($R^2 = 0.999$). The dotted and dashed lines represent the power law with exponent 1/3 and 1/12, respectively.

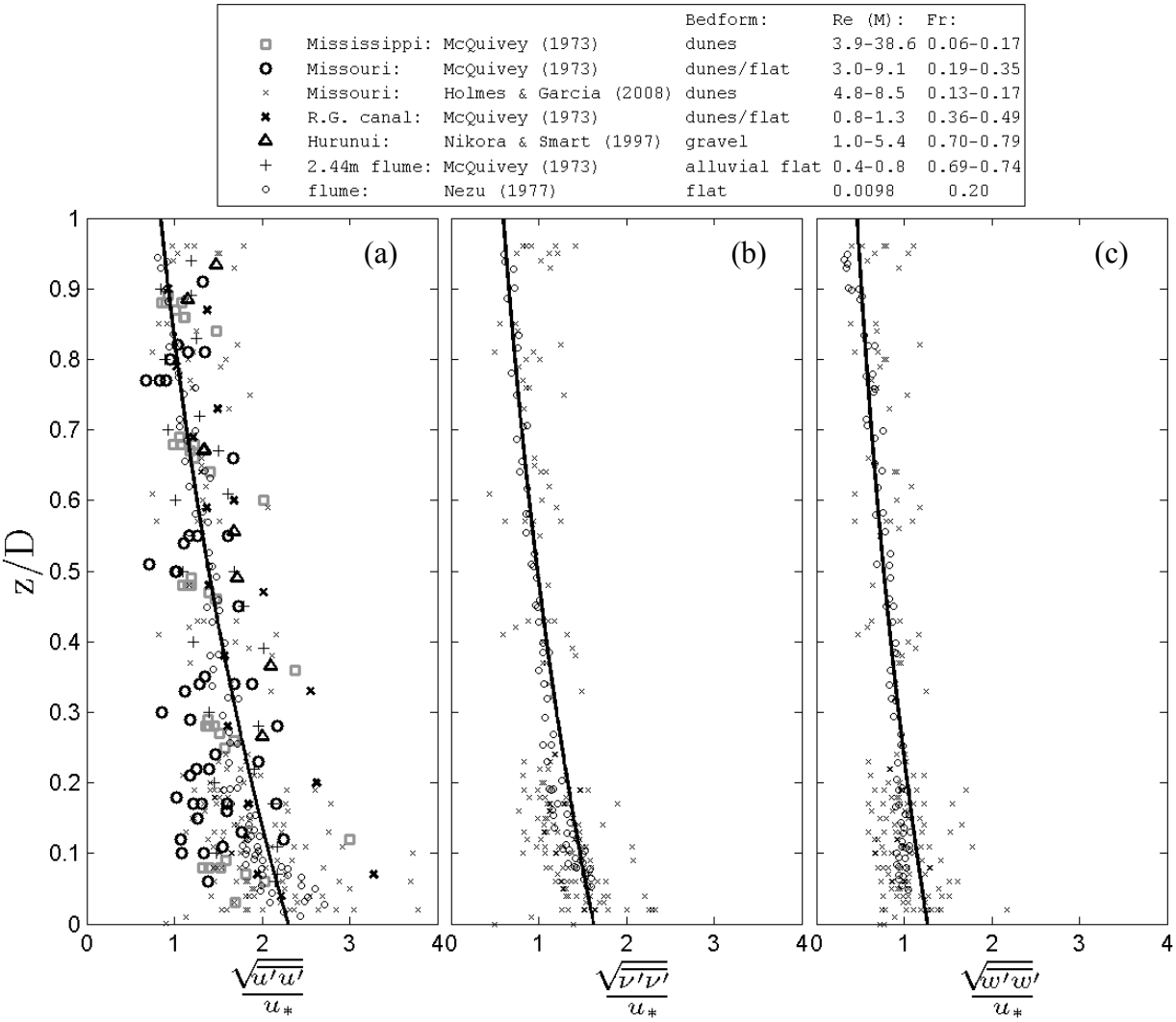

Figure 7. Exponential decay law profiles by Nezu and Nakagawa (1993) compared to field measurements, with *z* normalized by *D* and normal stresses, e.g. $\sqrt{\overline{u'u'}}$ normalized by shear velocity $u_* = \sqrt{\tau_o / \rho}$.

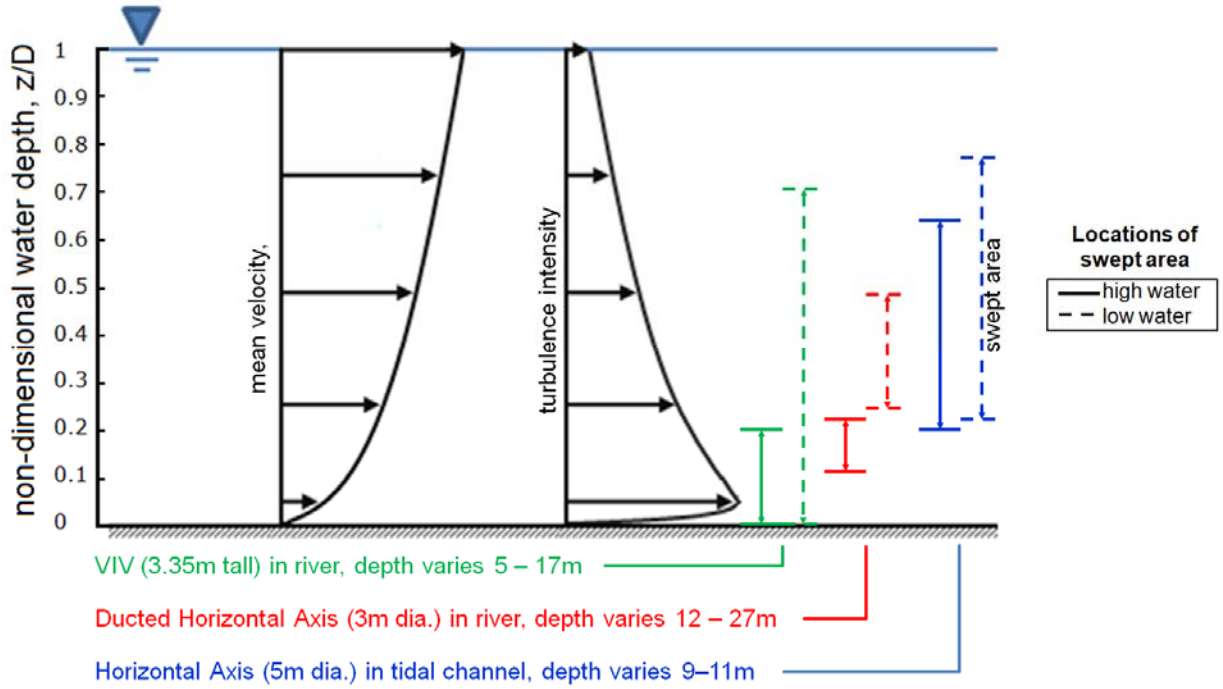

Figure 8. Effects of large depth variability on the location of the swept area (energy extraction area) relative to the velocity and turbulence profiles.